Chapter 5

Does Wnt disruption mediate immune exclusion?

5.1 Introduction

The capacity to avoid immune clearance is vital for cancer emergence and progression. Immune exclusion is defined as the capacity to keep immune populations out of the vicinity of the tumours[196]. This property has been linked to WNT activation across malignancies and specifically in colorectal cancer (CRC)[199, 182]. The first molecular mechanism relating WNT activation and T cell exclusion was described in the context of melanoma, where repression of *Ccl4* in neoplastic cells lead to defects in the recruitment of cross-presenting Batf3+ dendritic cells, with a subsequent decrease of Cd8+ T cell infiltration into the tumours[197]. Since then, further research has tried to unveil the intricacies of WNT-driven immune exclusion[194, 193], but the mechanisms by which this phenomena operates in CRC are far from understood.

Stem Cells (SC) possess cell-intrinsic characteristics that enable them to escape immune detection, a capacity which has been coined as Immune Privilege (IP)[14]. Given its role in the regulation of SC identity, it could be that WNT activation is mediating some of the immune evasion properties associated to stemness, which might be co-opted in the context of cancer.

As we saw in Chapter 3, the SC composition across malignant and pre-malignant lesions is not homogeneous. But does the stem/progenitor composition (i.e. Crypt Base Columnar -CBC-, Regenerative Stem Cells -RSC-, Transit Amplifying -TA- progenitors) of a lesion affect immune cell recruitment? Furthermore, although Wnt activation appears to be an almost ubiquitous requirement in CRC, the way in which different lesions acquire it varies across histological and molecular subtypes. Indeed, as previously explained, colorectal lesions can be divided in ligand-dependent (LD)

or ligand-independent (LI) according to whether WNT dysregulation occurs above or below the Frizzled receptor respectively[140]. But does the type of WNT alteration (i.e. LD or LI) that a tumour acquires impact its immune landscape?

Here, animal models of WNT disruption are used to explore the link between WNT activation and immune exclusion in the intestine. Moreover, pharmacological WNT inhibition is used to test whether T cell exclusion can be reverted in LD models of WNT-driven polyposis, and to investigate the molecular mechanisms by which WNT may be mediating these effects.

5.2 Objectives

- To assess the levels of immune infiltration across mouse models of WNT-driven transformation
- To study whether alternative pools of SC/progenitor cells drive a different re-arrangement of the immune populations within colorectal lesions.
- To assess whether LD and LI WNT alterations have distinct effects on the immune landscape of colorectal lesions.
- To investigate a possible mechanisms by which WNT activation may be hampering immune recruitment in mouse models of WNT-driven transformation.

5.3 T Lymphocytes are Distributed Unevenly Across the Crypt-Villus Axis

Expression of the T-cell Receptor (TCR) is a defining property of the T cell lineage. Cd3 is a component of the TCR complex which is commonly used to trace T lymphocytes in histopathological samples[242]. Here, Immunohistochemistry (IHC) for this marker was performed to provide a general overlook of the distribution of T lymphocytes in the intestines of WT animals. As described by Takashima et al[15], differences in the levels of Cd3+ cells were observed between the crypt and villi compartments. In particular, no Cd3+ Intraepithelial lymphocytes (IELs) were detected within the epithelium of the crypts (Fig.30A-C).

In order to provide a more comprehensive characterisation of the distribution of immune cells along the crypt-villus axis, Multiplex Immunofluorescence for a panel of common epithelial and immune markers (Epcam, Cd4, Cd8, Foxp3 and Cd68) was

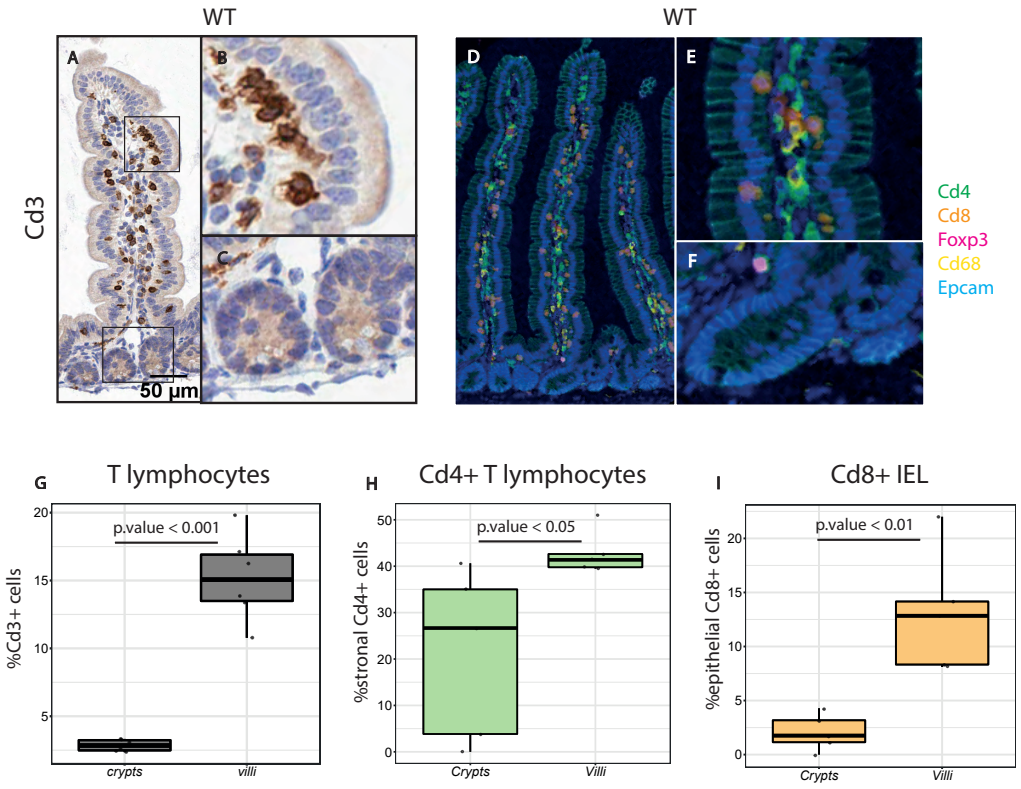

Figure 30: CBC cells present an immune exclusion phenotype. A-C. IHC for Cd3+ along the crypt villus axis of a WT mouse. C and D show details of the villi and crypt compartment respectively. D-F. Immune characterization of a WT crypt-villus structure using Multiplex Immunofluorescence (MPI) for a panel of antibodies: Cd4 (green), Cd8 (orange), Foxp3 (pink), Cd68 (yellow), Epcam (cyan), DAPI (blue). E and F show details of the villi and crypt compartment respectively. G-I. Image quantification of the numbers of T lymphocytes (G), Cd4+ T cells (H) and Cd8+ IEL (I) in crypts and villi of WT animals. Brown IHC was quantified using Qupath. MPI images were quantified using HALO. Differences between groups were analysed using a two-way t-test. Asterisks indicate a p-value <0.05 (*), <0.01(**) or <0.001 (***).

performed. Analysis of the immune subsets revealed a decrease of Cd8+ Intraepithelial lymphocytes (IELs) and Cd4+ stromal T cells in crypts of WT animals versus the villi, suggesting that the adaptive immune compartment was under-represented in this region (Fig.30D-I).

To investigate whether the epithelial cells themselves might be playing a role in the observed lymphocytic exclusion, the epithelium of the crypt and villi compartments were characterized at a transcriptomic level. As expected, enrichment for a

Wnt signature[128] was observed in the crypt epithelium with respect to the villi (Fig.31A). Furthermore, pathways related to the cell cycle, DNA replication and transcription/translation were also enriched in the crypt compartment, which was to be expected from a highly proliferative and biosynthetically active compartment. Contrarily, there was a clear downregulation of immune signatures in the crypt epithelium of WT animals with respect to villi, which suggests that the lack of Cd3+ cells may be part of a more general immune suppression phenotype (Fig.31B).

Among the immune processes which were downregulated in the crypts, *MHC-I mediated antigen presentation* ranked high in the list. Indeed, the expression of genes that code for MHC-I molecules (*H2-D1, H2-K1, B2m*) and antigen presenting machinery (*Tap2, Tapbp*) was lower in crypts than in villi (Fig.31C). Moreover, pathways involved in the activation of an adaptive immune response also ranked lower in the crypts (eg. *TCR signaling, Costimulation through the CD28 family*) (Fig.31B). These results suggest that the crypt epithelial cells might be less likely to present intracellular antigens to T cells and activate a CD8+ cytotoxic response.

Moreover, there was a difference in the types of cytokines and chemokines produced by the epithelium of the crypt and villi compartments. Chemokines are a type of molecules heavily involved in the migration of immune cells towards peripheral tissues. In particular, Cxcr3 is a chemokine receptor found in the surface of T, Natural killer, Natural killer T, B and dendritic cells which, upon interaction with its ligands cxcl9/10/11, drives the recruitment of immune cells to areas of Th1-induced inflammation[243]. A close look at the ligands that were differentially expressed along the crypt-villus axis revealed *Cxcl9-11* to be downregulated in the crypts (Fig.31D). Importantly, the expression of these ligands is regulated by innate pathways like NF-κb, Interferon(IFN)-γ and Toll-Like Receptors (TLR), which were repressed in the crypt compartment with respect to the villi (Fig.31B). In addition to *Cxcl9-11*, the transcription of other chemokines (i.e *Cxc3cl1, Ccl5, Ccl3* and *Xcl1*) was found to be decreased in the crypts (Fig.31D). Overall, lower expression of chemoattractants may contribute to the limited recruitment of immune cells towards the crypt compartment.

These observations suggest that there is immune modulating transcriptional variation along the crypt-villus axis in homeostatic murine small intestine. Although these changes correlate with established Wnt ligand gradients, proof of connection or causality was missing.

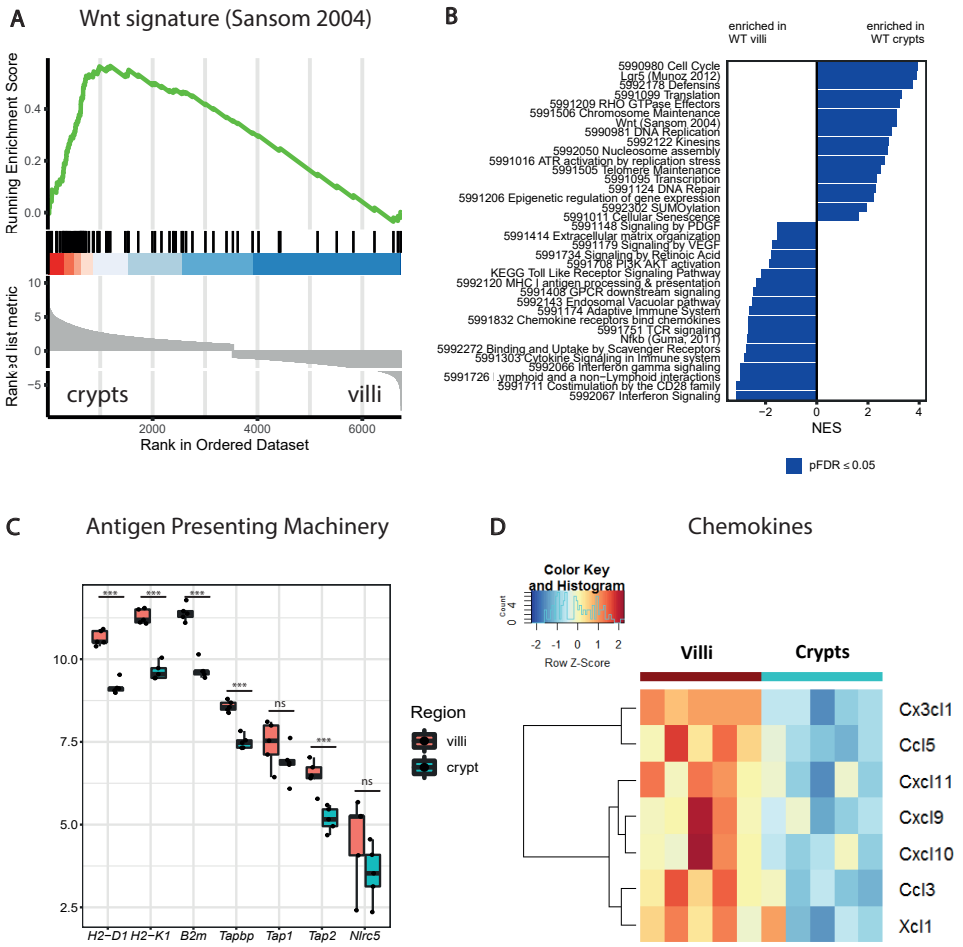

Figure 31: Immune processes are downregulated in the crypt compartment of WT animals. A. Gene Set Enrichment Analysis (GSEA) plot showing the enrichment of a WNT pathway[128] in crypts versus villi of WT animals. B. Pathways and processes which are Differentially Expressed (DE) between crypts and villi from WT animals. C. Boxplot showing the logCPM expression values for Antigen Presenting Genes in crypts and villi of WT animals. D. Boxplot representing the relative expression of DE chemokines between crypts and villi from WT animals. For GSEA, pathways were ranked by Negative normalized Enrichment Score. Statistical differences were assessed by the fast algorithm[232] and significance threshold was set at an adjusted p.value < 0.05. For logCPM values, significance was assessed using a pairwise t-test and p.value was adjusted using the Holm method. Asterisks indicating a p-value <0.05 (*), <0.01(**) or <0.001 (***).

5.4 Animal Models of WNT Disruption

To investigate the possible link between WNT activation and immune exclusion, mouse models of WNT disruption were used. As mentioned before, WNT alterations

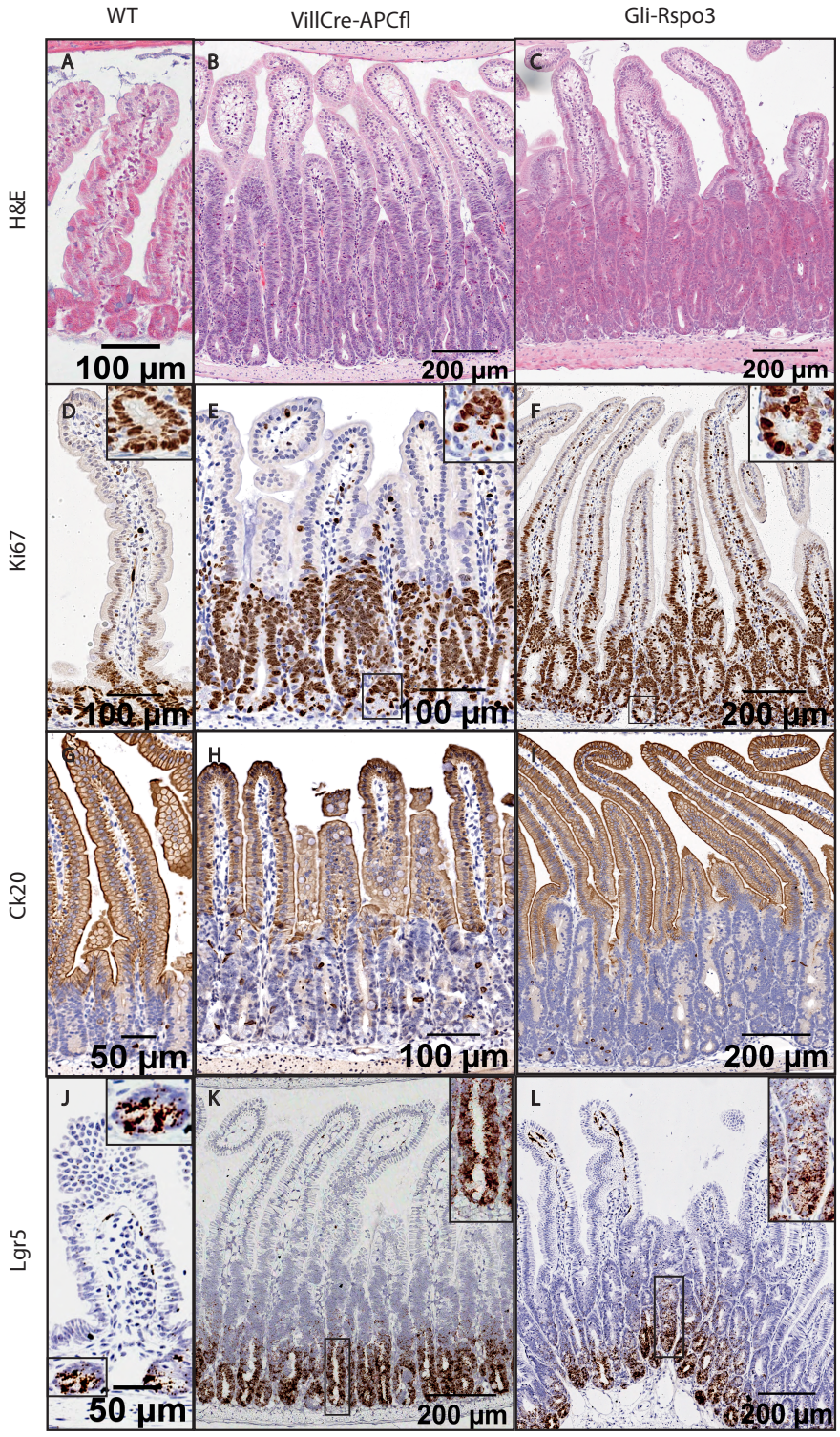

Figure 32: VilER-Cre-Apc$^{fl/fl}$ and Gli-Rspo3 animals present with an hyperproliferative phenotype. A-C. H&E of intestines from WT (A), *VilER-Cre-Apc*$^{fl/fl}$ (B) and *Gli-Rspo3* (C) mice. D-I. IHC for Ki67 (D-F) and Ck20 (G-I) in intestines from WT (D,G), *VilER-Cre-Apc*$^{fl/fl}$ (E,H) and *Gli-Rspo3* (F,I) mice. J-L. ISH for *Lgr5* in intestines from WT (J), *VilER-Cre-Apc*$^{fl/fl}$ (K) and *Gli-Rspo3* (L) mice.

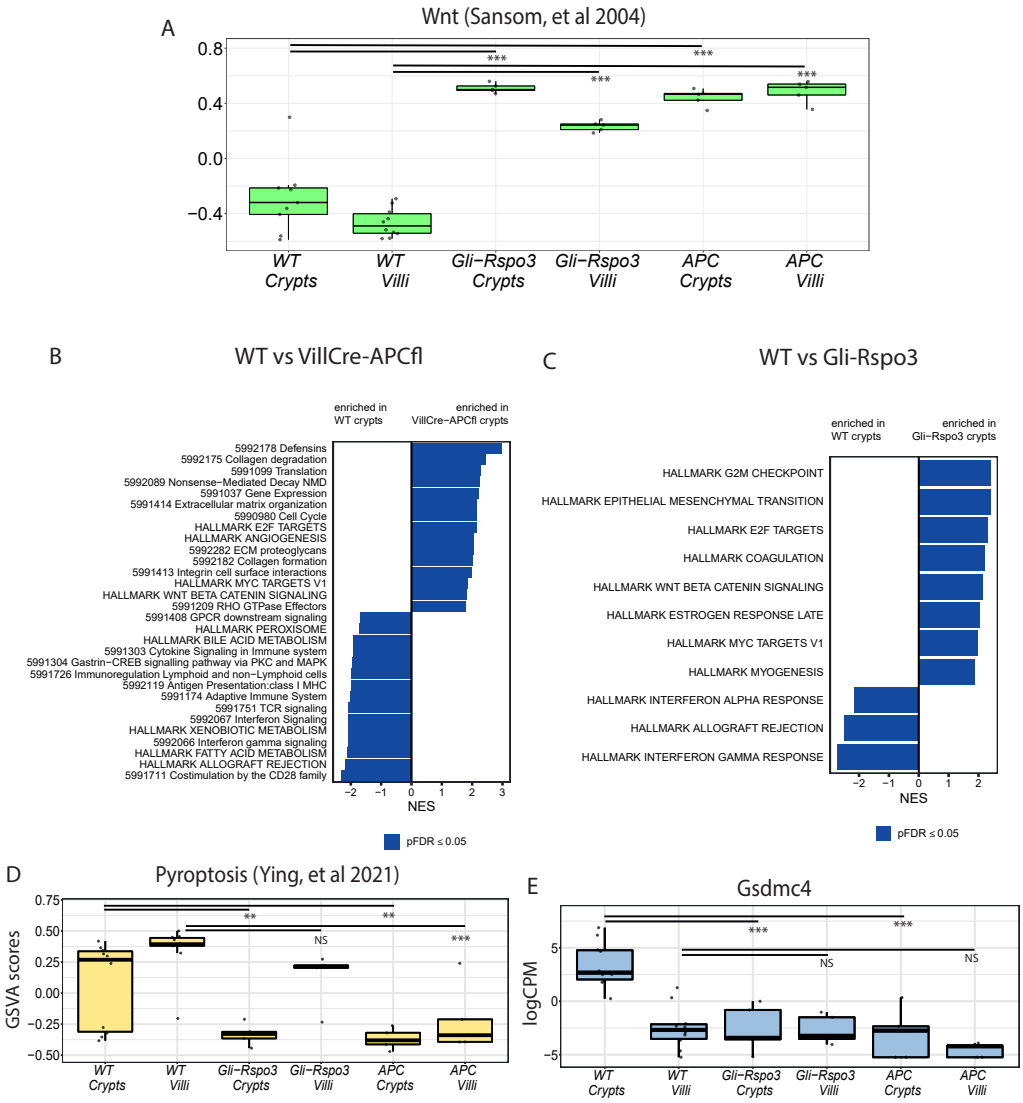

Figure 33: WNT disruption drives the downrwegulation of immune pathways and pyroptosis. A. GSVA scores for the WNT pathway in villi and crypt from WT, *VilER-Cre-Apc*$^{fl/fl}$ and *Gli-Rspo3* mice. B,C. Differentially expressed pathways between crypts of WT and *VilER-Cre-Apc*$^{fl/fl}$ (B) or *Gli-Rspo3* (C) animals. D,E. GSVA scores for pyroptosis (D) and logCPM values for *Gsdmc4* (E) in villi and crypt from WT, *VilER-Cre-Apc*$^{fl/fl}$ and *Gli-Rspo3* mice. Statistical significance was assessed using a pairwise t-test and p.value was adjusted using the Holm method. Asterisks indicate a p-value <0.05 (*), <0.01(**) or <0.001 (***)

can be classified as LD or LI based on whether they occur above or below the Frizzled receptor [140]. In order to model these two categories, animals of different genetic backgrounds were selected. The first of these animal models was the *Gli-Rspo3* mouse,

a LD model of Wnt-driven polyposis produced by introduction of the *Rspo3* gene in an inverse orientation between two pairs of *Lox* sites and behind the constitutive promoter *CAGGS*[142]. In these animals, tamoxifen-induced activation of the Gli-CreER^{T2} recombinase causes the inversion of the *Rspo3* gene in *Gli+* fibroblasts. The second model was the *VilER-Cre-Apc$^{fl/fl}$* mouse, a LI model which presents a conditional epithelial homozygous deletion in the *APC* gene. Upon tamoxifen injection, both mouse models developed a comparable hyper-proliferative phenotype (Fig.32A-C), with a consequent increase in proliferative Ki67+ (Fig.32D-F) cells and a reduction in functional differentiated Cytokeratin 20(Ck20)+ enterocytes (Fig.32G-I). Furthermore, both models experience an expansion of the *Lgr5+* CBC compartment (Fig.32J-L). Importantly, *Gli-Rspo3* and *VilER-Cre-Apc$^{fl/fl}$* animals have a life-span of five days from the day of the last injection, a time by which they have developed signs of pathology like anaemia, diarrhoea, inactivity and hunching.

To investigate the effects of WNT activation on the epithelium, this compartment was collected from the crypt and villi of *Gli-Rspo3* and *VilER-Cre-Apc$^{fl/fl}$* animals, and RNA was extracted and submitted for RNA sequencing (See Chapter2). As expected, the WNT pathway was enriched in crypts versus villi in WT mice, and was generally higher in WNT-disrupted models with respect to WT mice (Fig.33A). Moreover, immune pathways appeared to be downregulated in *Gli-Rspo3* and *VilER-Cre-Apc$^{fl/fl}$* animals (Fig.33B,C), which is in accordance with previous studies [182]. Interestingly, a pyroptosis gene signature [244] was found to be downregulated across WNT-disrupted models (Fig.33E), suggesting that WNT may contribute to the regulation of this immunogenic type of cell death.

Pyroptosis is a cell death mechanism that entails the exposure of cell damage signals (DAMPS) and the release of pro-inflammatory molecules (Il-1β, Il-18), which can contribute to the activation and recruitment of immune populations[245]. Gasdermin is a family of pore-forming proteins that act as pyroptosis effectors. Among the list of differentially expressed genes, the levels of *Gsdmc4* were consistently lower in crypts of *Gli-Rspo3* and *VilER-Cre-Apc$^{fl/fl}$* animals when compared to WT (Fig.33D). Based on these observations, the following working hypothesis was established: it was possible that WNT was contributing to regulation of Pyroptosis at least partially through suppression of *Gsdmc4*.

All in all, *VilER-Cre-Apc$^{fl/fl}$* and *Gli-Rspo3* animals are good tools to study the short-time effects of a sudden and abrupt WNT activation. Upon recombination, these mice developed a profound intestinal hyperplasia which caused them to develop

signs of pathology within 5 days. Transformed epithelium presented high WNT activity, which came together with downregulation of immune pathways and repression of a pyroptosis signature. However, the short life-span of these animals does not allow to see how the epithelia-immune cell dynamics are altered in the context of a neoplastic lesion. To see whether these findings extended to neoplastic settings, alternative disease models were needed.

5.5 Animal Models of WNT-driven Polyposis

In WT intestines and models of abrupt WNT disruption, high WNT activation was associated to a downregulation of immune pathways. To explore whether these findings extended to clinically relevant models of colorectal polyposis, the APC^{Min}[203, 204] and the $Lgr5^{tm1(cre/ERT2)Cle}$-$Gt(Rosa)26Sortm^{6(CAG-Rspo3)Nki}$/A (*Lgr5-Rspo3*)[142] mice were used.

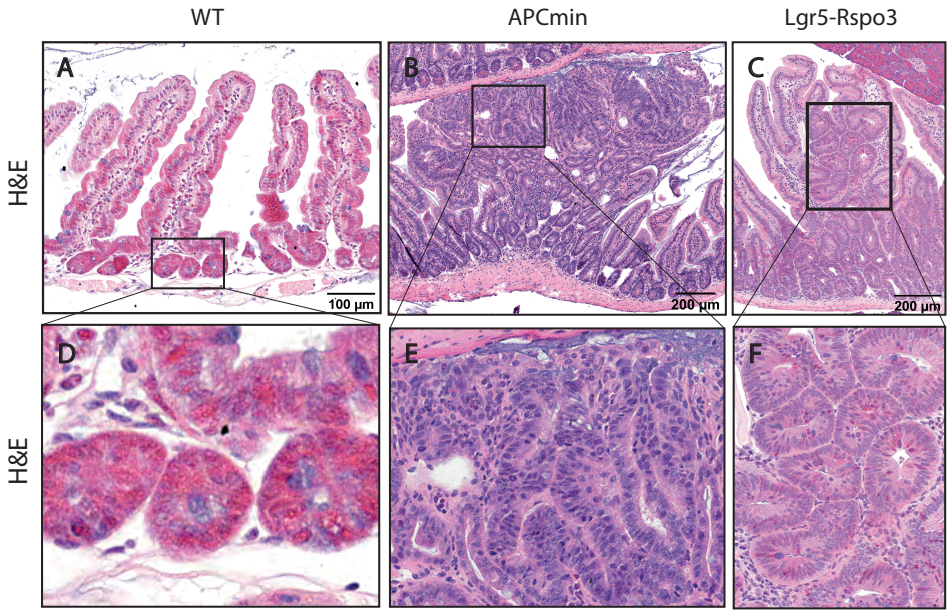

Figure 34: Histopathology ofAPC^{Min} and *Lgr5-Rspo3* polyps. A-F. H&E of WT intestines and polyps from APC^{Min} and *Lgr5-Rspo3* animals. D-E show details from conventional (D) and ectopic crypts (E,F).

The APC^{Min} mouse is a LI, constitutive model of APC-driven tumorigenesis which has an heterozygous truncating mutation at codon 850 of the *APC* gene. Sporadic loss or mutation of the reminding *APC* allele causes these animals to develop tumours in the intestine as well as other body regions (eg. mammary glands). The lifespan

of these animals is of approximately 200 days, and they develop on average 20 to 100 polyps throughout their intestinal track on a C57BL/6J background. APC^{Min} animals present polypoidal, sessile or papillary adenomas which size can reach 8mm, and with limited dysplastic features. These lesions can be found across the intestine, but they are more common in the small bowel than in the colon [203, 204] (Fig.34). Importantly, as discussed in Chapter 3, APC^{Min} animals have a Lgr5+ cell of origin, and their polyps are heavily populated by CBC.

The *Lgr5-Rspo3* mouse is a LD models of Wnt-driven polyposis produced by introduction of the *Rspo3* gene in an inverse orientation between two pairs of *Lox* sites and behind the constitutive promoter *CAGGS*[142] (Fig.34). In these animals, tamoxifen-induced activation of the Lgr5-CreER^{T2} recombinase causes the inversion of the *Rspo3* gene in cells that express *Lgr5*. Given that this mouse model had never been experimentally used in a C57Bl/6J background before, a detailed characterization was performed prior to its experimental use.

5.5.0.1 Phenotypic Characterization of the *Lgr5-Rspo3* Mouse

For phenotypic characterization, recombination was induced at the age of 6 weeks and samples were collected when the animals had developed signs of pathology (i.e. pale feet, hunching and diarrhoea), which occurred from 2 weeks to over 3 months post-injection.

Histopathological assessment of these samples revealed an hyperplastic phenotype across the small bowel which abruptly decreased when reaching the colon (Fig.35A-D). Furthermore, these animals presented adenomas in increased number but decreased size across the small bowel, and there were limited numbers of polyps in the colon (Fig.35E,F). Importantly, *Lgr5-Rspo3* polyps were characterized by the presence of ectopic crypts (ECF) and rarely showed signs of carcinogenic transformation (Fig.35).

IHC for Ki67 and Ck20 were used to monitor the proportion of proliferative and differentiated cells within the intestines of *Lgr5-Rspo3* animals respectively (Fig.36). Disruption of normally polarised R-spondin gradients impacted the sharp normal demarcation between proliferating and differentiating cells at the crypt villus axis of the homeostatic intestine, with the presence of aberrantly proliferating cells in ECF above the crypt-villus isthmus in Lgr5-Rspo mice. Interestingly, the percentage of Ki67+ cells in *Lgr5-Rspo3* crypts was reduced in comparison to their WT counterparts (Fig.36). This is in agreement with the observation by Hilkens et al that R-spondin 3 overexpression increased the number of quiescent cells in the crypts[142].

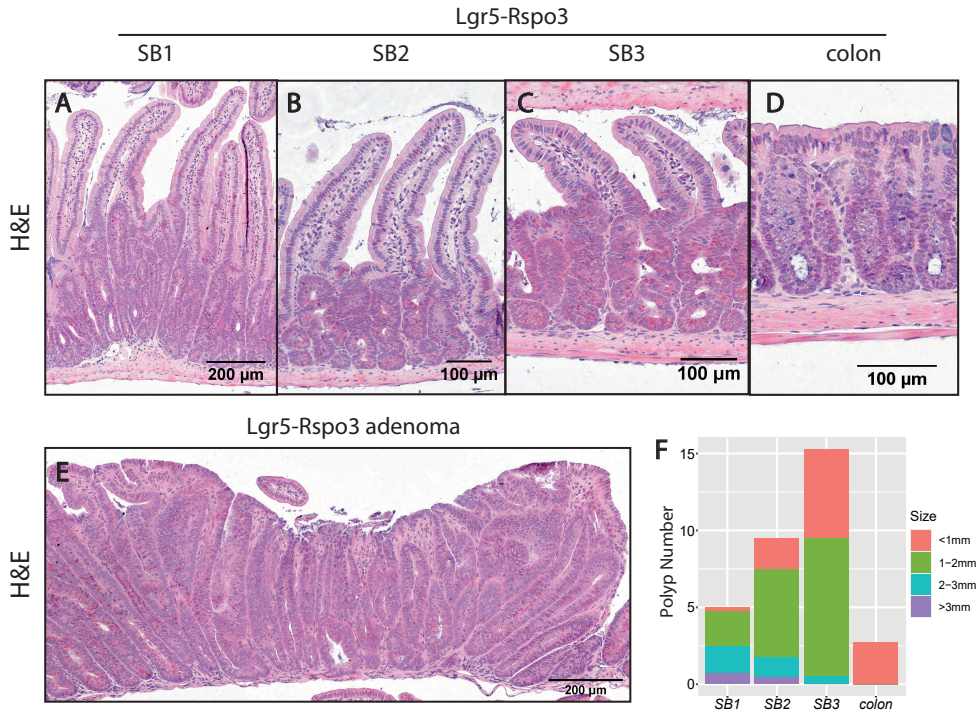

Figure 35: Histopathology of *Lgr5-Rspo3* samples. A-E. H&E stains showing SB1 (A), SB2 (B), SB3 (C) and colon (D) regions as well as polyps (E) of *Lgr5-Rspo3* animals. F. Stacked barplot showing the number and size of polyps in the SB1, SB2, SB3 and colon regions from *Lgr5-Rspo3* intestines (n = 5).

Overall, the percentage of Lgr5+ cells was increased in these animals, although the expression of this transcript was almost exclusively localized to conventional crypts, whereas hyper-proliferative areas within the villi and most ECF were *Lgr5-* (Fig.37A-E). Moreover, fluorescent *In situ hybridization* (ISH) for *Lgr5* and *Rspo3* revealed streams of *Lgr5-, Rspo3+* cells migrating upwards from the base of the crypts, suggesting that *Rspo3* overexpression is insufficient to maintain *Lgr5* expression, which may also require a high Wnt environment. Consequently, recombinant cells may lose their CBC identity as they migrate up the villi walls, due to the decreasing Wnt gradient. Interestingly, some hyperplastic crypts did not express *Rspo3*, which indicates that R-spondin3 has both autocrine and paracrine effects in the intestine of *Lgr5-Rspo3* animals. Furthermore, some basal crypts appeared to have been completely taken over by recombinant cells, whereas others had foci of *Rspo3+* progenitors but remained mostly *Lgr5+, Rspo3-* (Fig.37B). In their publication, Hilkens et al described an increase in the number of Lgr5+ quiescent cells in the conventional crypts of *Lgr5-Rspo3* animals. Indeed, lineage tracing of Lgr5+ progenitors revealed a sharp decrease in the number of ribbons observed in these mice with respect to con-

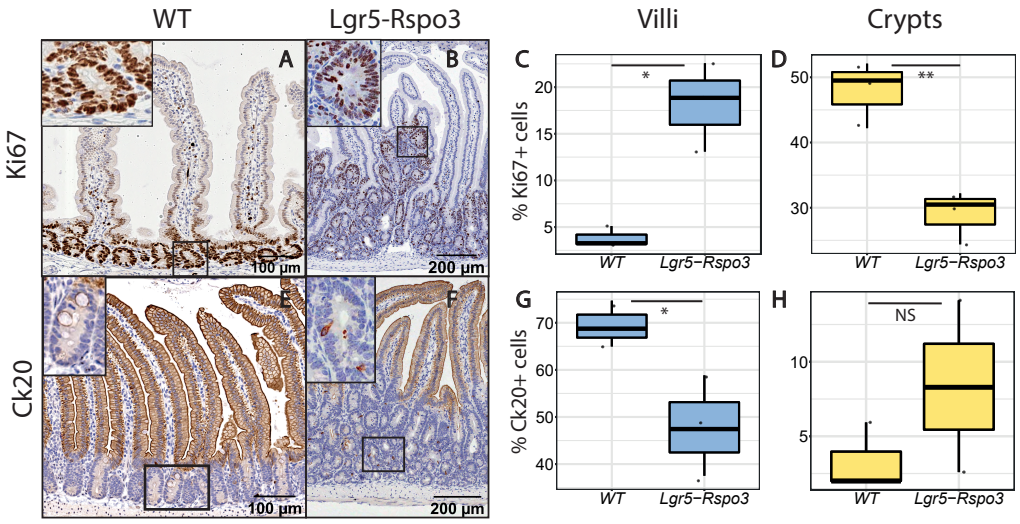

Figure 36: Remodelling of the proliferative and differentiated compartments in *Lgr5-Rspo3* animals. A,B,E,F. IHC for the markers Ki67 (A,B) and Ck20 (E,F) in WT (A,E) and *Lgr5-Rspo3* (B,F) intestines. Details show conventional (A,E,F) and ectopic crypts (B). C,D,G,H. Boxplots showing the percentage of Ki67+ (C,D) and Ck20+ (G,H) cells in villi (C,G) and crypts (D,H) of WT and *Lgr5-Rspo3* animals. Brown IHC was quantified using Qupath. Significance was assessed using a one-sided t-test and p.value was adjusted using the Holm method. Asterisks indicating a p-value <0.05 (*), <0.01(**) or <0.001 (***).

trols[142]. The capacity of Rspo ligands to stop Lgr5+ cells from leaving the crypt was described and coined as crypt "trapping" by Yan et al [64]. Collectively, these results seem to indicate that a proportion of CBC within the *Lgr5-Rspo3* crypts may indeed be trapped and unable to expand.

The expression of Frizzled (Fzd) and Lgr receptors is heavily regionalized along the crypt-villus axis: CBC are positive for *Fzd7* and *Lgr5*, whereas TA progenitors express *Fzd5* and *Lgr4* instead[237, 246]. ISH for *Lgr4* revealed a profound upregulation of this transcript in *Lgr5-Rspo3* intestines (Fig.37R-U), which had also been previously described by Hilkens et al[142], and which came together with increased expression of *Fzd5* (Fig.37N-Q). Indeed, all the hyperplastic and polypoid structures in the intestines of these animals were positive for both *Lgr4* and *Fzd5*. This data suggests that *Lgr4* and *Lgr5* may be subjected to different regulatory mechanisms, which could be indicative of non-redundant roles in the transduction of Wnt ligands. At least in this model, *Lgr5-* progenitors seem to be responding to Rspo3 overexpression via their Lgr4 receptors, which drives the hyper-proliferative and ECF phenotype observed in *Lgr5-Rspo3* animals.

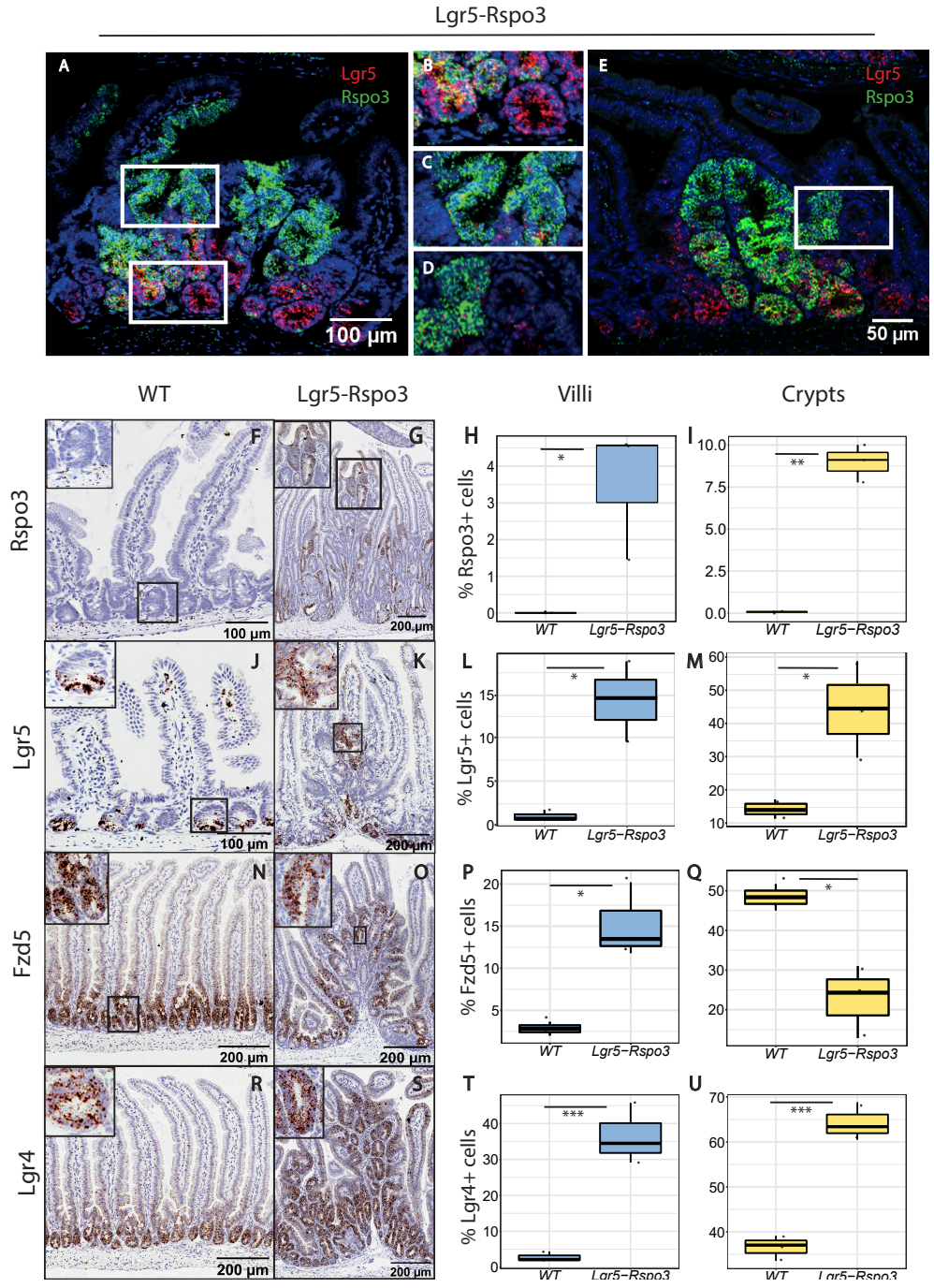

Figure 37: There is an expansion of *Lgr4+,Fzd5+* cells in the intestines of *Lgr5-Rspo3* animals. A-E. Fluorescent ISH for the markers *Lgr5* and *Rspo3* in intestinal sections from *Lgr5-Rspo3* animals. B-D show details of conventional (B) and ectopic crypts (C,D). F,G,J,K,N,O,R,S. Single-channel ISH for the markers *Rspo3* (F,G) *Lgr5* (J,K), *Fzd5* (N,O) and *Lgr4* (R,S) in WT (F,J,N,R) and *Lgr5-Rspo3* (G,K,O,S) intestines. Boxplots showing the percentage of*Rspo3+* (H,I) *Lgr5+* (L,M), *Fzd5+* (P,Q) and *Lgr4+* (T,U) in villi (H,L,P,T) and crypts (I,M,Q,U) of WT and *Lgr5-Rspo3* animals. Significance was assessed using a one-sided t-test and p.value was adjusted using the Holm method. Asterisks indicate a p-value <0.05 (*), <0.01(**) or <0.001 (***).

A recent study by Flanagan et al demonstrated that APC mutations are selected within the CBC compartment via supercompetition and effective niche succession [234]. Contrarily, overexpression of *Rspo3* seems to drive a "crypt-trapping" phenotype in *Lgr5-Rspo3* animals, whereas it favours the preferential expansion of *Lgr5-*, *Lgr4+* progenitors [142]. Hence, the mechanism by which WNT disruption occurs may affect the cell by which colorectal transformation originates. However, whether this conditions the immune environment of the lesions was unknown at this stage.

5.6 Immune Characterization of *Lgr5-Rspo3* and APC^{Min} Animals

In order to assess the levels of T cell infiltration in animal models of Wnt-driven polyposis, IHC for Cd3 was performed in sections of *Lgr5-Rspo3* and APC^{Min} intestines. Overall, the polyps of both models and the hyperplastic compartment of *Lgr5-Rspo3* mice showed decreased levels of Cd3+ cells with respect to the villi, similarly to the crypts within WT intestines. In particular, the epithelium of these compartment showed no signs of T cell infiltration, whereas some lymphocytes could be observed in the lamina propria (Fig.38).

Next, a more comprehensive characterisation of the immune landscape of these animals was performed using Multiplex Immunofluorescence for a panel of common epithelial and immune markers (Epcam, Cd4, Cd8, Foxp3 and Cd68) (Fig.39), which confirmed the findings of differential T cell infiltration originally identified with the Cd3 marker. Generally, the polyps and crypts of APC^{Min} and *Lgr5-Rspo3* animals tended to have lower levels Cd8+ T lymphocytes and macrophages, and more Foxp3+ T cells than the untransformed villi (Fig.39C-F. I-L). Unlike the polyps of APC^{Min} animals, *Lgr5-Rspo3* lesions have a mixed composition, with areas of ectopic crypt formation which acquire normal-looking characteristics as they approached the edges of the polyp. This may be the reason why, despite the similar trends observed within both models, the differences between compartments did not reach statistical significance in *Lgr5-Rspo3* mice. Importantly, in this last model, the sharpest differences were noted within ECF regions (Fig.39).

Overall, these results suggest that the immune exclusion phenotype observed in WT crypts is extended to areas of early transformation within models of WNT-driven polyposis. Importantly, immune exclusion was not limited to lesions populated by CBC, but also found in *Lgr5-Rspo3* polyps, which are driven by an expansion of

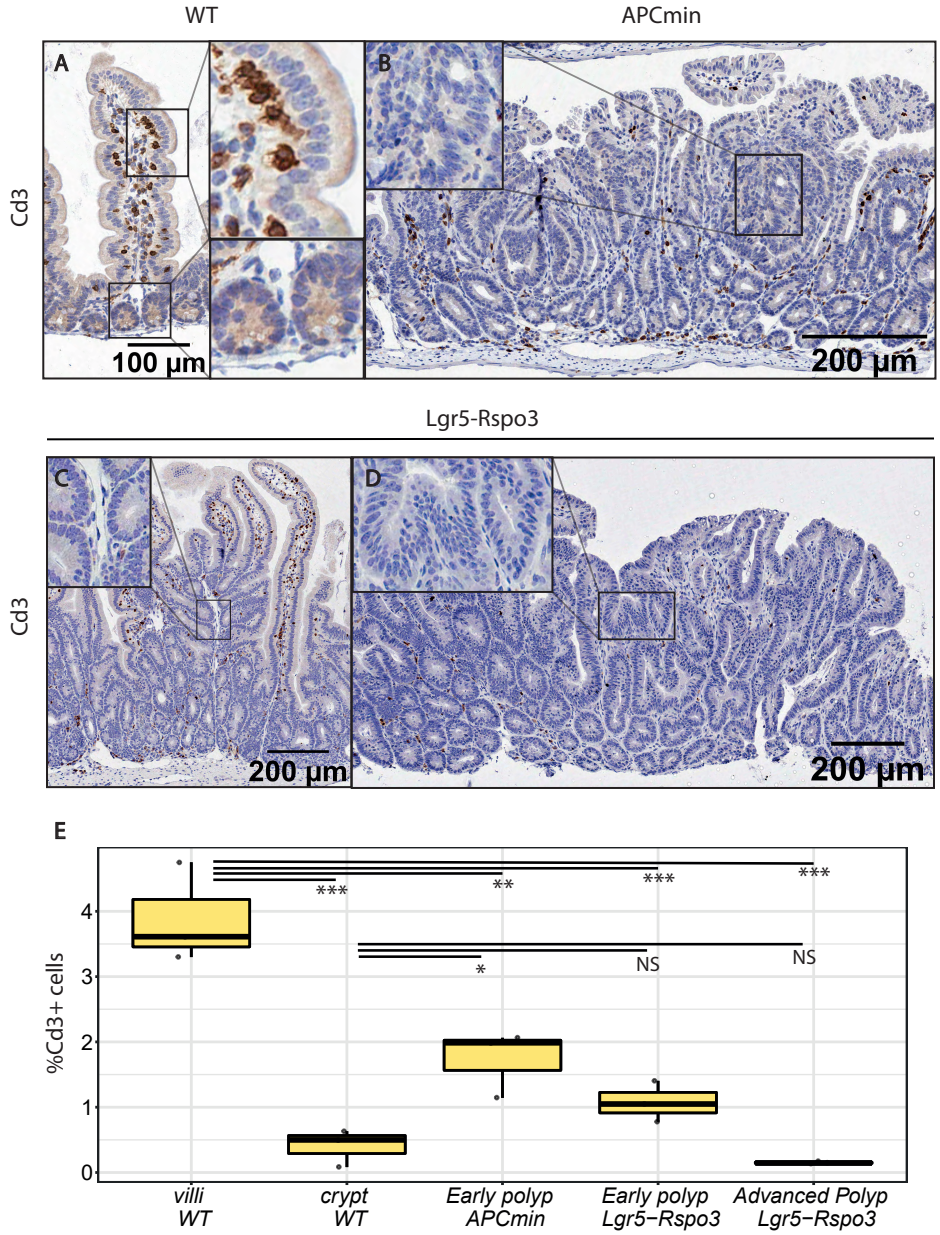

Figure 38: T cell infiltration in mouse models of Ligand-Dependent and Ligand-Independent WNT disruption. A-D. IHC for Cd3 in intestines from WT animals and polyps from APC^{Min} and *Lgr5-Rspo3* mice. E. Boxplot showing the percentage of Cd3+ cells in WT, APC^{Min} and *Lgr5-Rspo3* tissues. Brown IHC was quantified using Qupath. Significance was assessed using a pairwise t-test and p.value was adjusted using the Holm method. Asterisks indicate a p-value <0.05 (*), <0.01(**) or <0.001 (***).

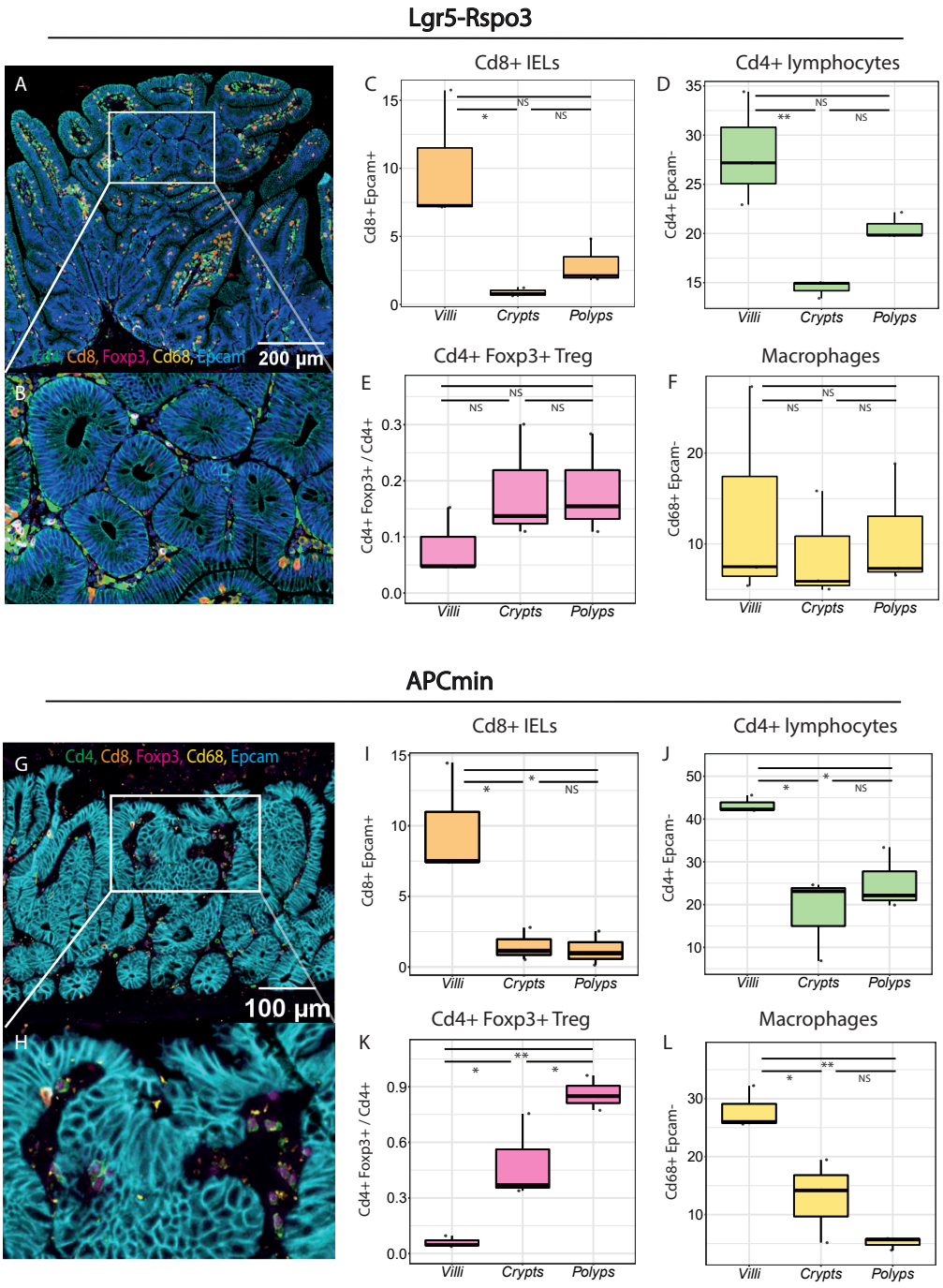

Figure 39: Immune characterization of APC^{Min} and *Lgr5-Rspo3* polyps using Multiplex Immunofluorescence (MPI) for a panel of antibodies: Cd4 (green), Cd8 (orange), Foxp3 (pink), Cd68 (yellow), Epcam (cyan), DAPI (blue). C-F,I-L. Image quantification of the numbers of Cd8+ IELs (C,I), Cd4+ T cells (D,J), Cd4+Foxp3+ regulatory T cells (E,K) and Cd68+ macrophages (F,L) in MPI images from *Lgr5-Rspo3* (C,D,E,F) and APC^{Min} (I,J,K,L) using HALO. Significance was assessed using a pairwise t-test and Holm correction applied. Asterisks indicate a p-value <0.05 (*), <0.01(**) or <0.001 (***).

Lgr5- progenitors. However, whether the immune exclusion mechanisms in these two models are equivalent remained unanswered.

5.7 Lgr5+ Cell Ablation Mildly Changes the Cd3+ Composition of APC^{Min} Polyps

The previous results suggested that TA and CBC cells have comparable levels of IP. To confirm whether this property was conserved upon changes in the SC composition, the *Lgr5-CreER*^{ER}*-DTR- APC*^{Min} (*APC*^{Min}*-Lgr5*^{DTR}) mouse model was used. As previously described in Chapter 3, these animals express the *Diphteria Toxin(DT) Receptor* under the inducible epithelial promoter *Lgr5-Cre*, which renders them susceptible to CBC ablation upon DT administration. Importantly, *APC*^{Min} polyps are completely repopulated by Anxa1+ RSC 24h post-injection, although CBC gradually reappear reaching normal levels 5 days after DT treatment (see Chapter 3).

APC^{Min}*-Lgr5*^{DTR} mice were injected at ages ranging from 80-150 days, a time by which they had developed polyps, and samples were collected 24h, 3 days and 5 days after DT injection. ISH for *Lgr5* evidenced the sharp reduction in the number of CBC 24h post-injection, which were recovered by day 5 (Fig.40A-D,I). Furthermore, IHC for Cd3 showed no differences between controls and *APC*^{Min}*-Lgr5*^{DTR} 24h and 3d post-injection (Fig.40E-H,J).

Next, RNAseq counts for samples collected 24h and 5 days (Chapter3) were used to investigate changes in the immune characteristics between samples. The Stem Cell Index values increased 24h after DT administration but were recovered by day 5 (Fig.41A), which matched the trend observed in the histopathological sections. Moreover, the levels of expression of *Prf1* and *Gzmb* were used as a surrogate of cytotoxic activity, as described by Rooney et al [247]. Briefly, the geometric mean of these values was calculated and compared across conditions, but no changes were observed 24h post-injection (Fig.41B). As expected, upregulation inflammatory pathways followed the acquisition of a RSC phenotype (24h), but these pathways returned to control levels when CBC reappeared (day 5) (Fig.41C,D).

Interestingly, a subtle increase in the numbers of Cd3+ T cell was detected 5 days after DT administration (Fig.40H,J). Importantly, this phenomena seemed to be restricted to specific areas within the *APC*^{Min}*-Lgr5*^{DTR} polyps. Moreover, there was a significant increase in cytotoxic scores 5 days after injection with respect to control levels (Fig.41B). The reason for this late and subtle T cell infiltration is yet not clear.